

Impact of Localization Errors on Label Quality for Online HD Map Construction

Alexander Blumberg^{1*}, Jonas Merkert^{1*}, Richard Fehler², Fabian Immel²,
Frank Bieder², Jan-Hendrik Pauls¹ and Christoph Stiller¹

Abstract—High-definition (HD) maps are crucial for autonomous vehicles, but their creation and maintenance is very costly. This motivates the idea of online HD map construction. To provide a continuous large-scale stream of training data, existing HD maps can be used as labels for onboard sensor data from consumer vehicle fleets. However, compared to current, well curated HD map perception datasets, this fleet data suffers from localization errors, resulting in distorted map labels.

We introduce three kinds of localization errors, Ramp, Gaussian, and Perlin noise, to examine their influence on generated map labels. We train a variant of MapTRv2, a state-of-the-art online HD map construction model, on the Argoverse 2 dataset with various levels of localization errors and assess the degradation of model performance. Since localization errors affect distant labels more severely, but are also less significant to driving performance, we introduce a distance-based map construction metric. Our experiments reveal that localization noise affects the model performance significantly. We demonstrate that errors in heading angle exert a more substantial influence than position errors, as angle errors result in a greater distortion of labels as distance to the vehicle increases. Furthermore, we can demonstrate that the model benefits from non-distorted ground truth (GT) data and that the performance decreases more than linearly with the increase in noisy data. Our study additionally provides a qualitative evaluation of the extent to which localization errors influence the construction of HD maps.

Index Terms—HD Map Construction, Automated Driving, Chamfer Distance, Noisy Labels, Localization Error

I. INTRODUCTION

High-definition (HD) maps are a fundamental component of today’s autonomous vehicle architectures. In contrast to standard-definition (SD) navigation maps, HD maps contain more detailed, more precise and additional semantic information about the topology of the road network. However, HD map construction is done mainly with mobile mapping platforms or survey vehicles equipped with highly precise sensors and reference global navigation satellite system/inertial navigation system (GNSS/INS) units. For that reason, HD map generation and maintenance is costly and time-consuming. A novel idea is aiming to utilize machine learning methods to perceive and construct HD maps online from onboard sensor data [1], [2], [3], [4], [5].

*These authors contributed equally to this work.

¹Institute of Measurement and Control Systems, Karlsruhe Institute of Technology (KIT), Karlsruhe, Germany {alexander.blumberg, jonas.merkert, jan-hendrik.pauls, stiller}@kit.edu

²FZI Research Center for Information Technology, Karlsruhe, Germany {fehler, immel, bieder}@fzi.de

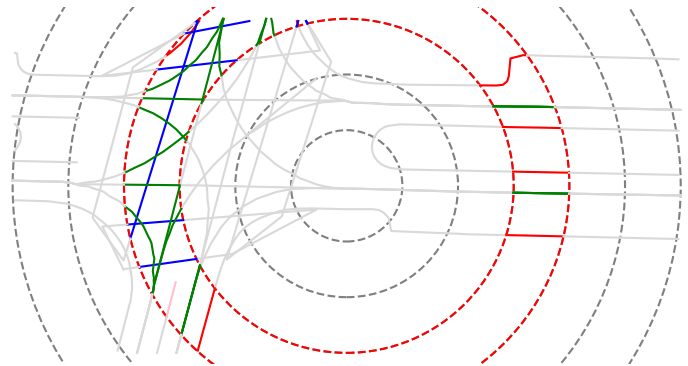


Fig. 1: Ring evaluation input (colored) over the entire scene (grey). Displayed are the map elements road boundaries (red), centerlines (green), pedestrian crossings (blue), and dividers (pink). Rings plotted as dashed with the currently observed ring (red) and other rings (grey).

Existing HD map construction datasets like Argoverse 2 [6] or nuScenes [7] utilize sensor data with high precision but are limited in size and diversity. While it is unclear how to scale the spatial extent of HD map coverage, existing vehicle fleets can provide a basically unlimited amount of sensor data. This data with high diversity in sensor setups and environment conditions, can be used as training data for online HD map construction when recorded in places with HD map coverage. However, their ego localization is less reliable, and the resulting vehicle poses are less accurate. This, in turn, leads to distorted HD map ground truth. For this reason, it is important to know, how localization errors affect ground truth quality, how this impairs online HD map construction performance, and hence, which level of precision the ego localization has to reach for HD map construction models to predict sufficiently precise maps.

The contributions of this work are:

- We are the first to model diverse localization noise based on real-world localization uncertainty patterns (Section III-A). For each of the three distortion types, we apply increasing levels of noise and apply it to a map perception dataset.
- We train a state-of-the-art online HD map construction model using the various distortions. This allows us to compare the degradation of model performance.

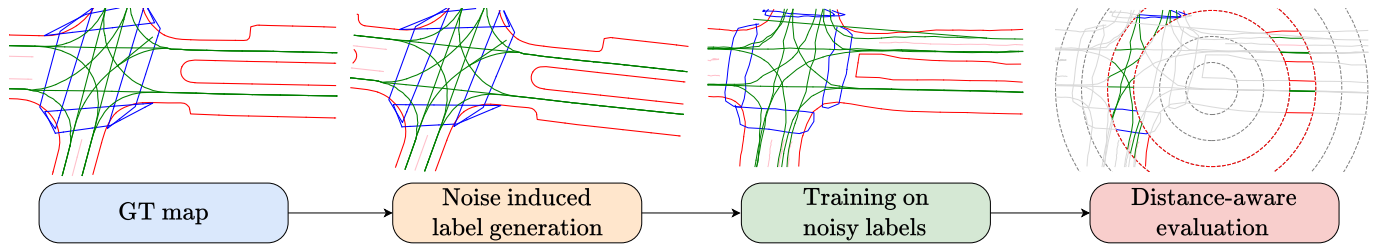


Fig. 2: Flowchart with an overview from map to evaluation. The noise application is described in Section III-A, details about the ground truth (GT) and training can be found in Section IV-A and we introduce our distance-aware evaluation metric in Section III-B.

- Since angular errors affect distant map elements more severely, we introduce a novel distance-aware map construction metric that evaluates label distortions and the model performance within different perception ranges (Section III-B).
- To examine the cause and effects, we compare original ground truth, distorted labels, and model predictions using the new distance-aware metric.

II. RELATED WORK

A. Online HD Map Construction

Today’s state-of-the-art HD Map Construction models utilize sensor data of the surrounding scene to predict vectorized map elements in their sparse polyline representation. Therefore, features are extracted from camera or LiDAR data and transformed into a bird’s-eye-view feature space. Subsequently, a Detection Transformer (DETR) [8] architecture predicts the vectorized map elements.

VectorMapNet [3] leverages a coarse-to-fine approach to predict the map elements in an autoregressive manner. In contrast, MapTR [1] and MapTRv2 [2] address the speed limitations of the autoregressive approach by introducing a new query design in the transformer decoder and treat the task as a point set prediction problem with a fixed number of points. Recent approaches have demonstrated significant improvements by taking advantage of previous predictions in a temporal or spatial manner [4], [5], [9]. Not only the inclusion of the temporal aspect is the subject of current research, but also the expansion of the sensor data to include additional prior information from existing SD navigation maps or older HD maps from previous drives [10], [11], [12].

B. Effect of noisy labels and sensor deviations

This work examines the impact of noisy labels during the training process on the outcome of online map construction. In recent years, the evaluation of label errors has garnered increased interest in the research community, and novel methods for classification and object detection tasks have been developed to handle noisy labels effectively [13], [14], [15]. Adhikari et al. [16] examine the effect of missing labels in object detection and therefore remove a percentage of bounding box labels during training. Besides missing labels, Freire et al. [17] and Zhu et al. [18] also explore the impact of

incorrect or imprecise labels, such as class shifts or bounding box distortions.

In addition to investigating the issue of noisy labels in object detection, research in online HD map construction also examines the impact of erroneous or poor-quality data. MultiCorrupt [19] and MapBench [20] evaluate the effect of weather conditions, sensor failures, or motion blur. Conversely, MapTR [1], [2] explores the impact of camera deviations on map construction, such as a shift of the camera position or calibration errors. The aforementioned studies investigate the effect of noise on the input and validation data. In contrast, our research focuses on the impact of noisy map labels during training, arising from localization and heading errors, on the performance of the model. The related work section listed above shows that there are no comparable studies to date.

III. METHODOLOGY

A. Noise types

We include three different noise cases Ramp, Gaussian and Perlin noise, for which we each calculate an altered position $x_\eta(t)$, $y_\eta(t)$ and orientation $\theta_\eta(t)$ based on the original pose $x_{gt}(t)$, $y_{gt}(t)$ and $\theta_{gt}(t)$.

1) *Ramp noise*: A vehicle’s localization module may fuse input from various sources such as GNSS, IMU, magnetometer, wheel odometry, visual localization, etc. Based on a vehicle dynamic model such, as the single-track model [21] and a filter such as an Extended Kalman filter this module will return a combined localization output. This allows for limiting the downsides of certain localization means such as higher noise levels for GNSS localization of drifting properties for IMU and wheel odometry-based approaches.

Effects such as blockage of the GNSS signal, whether it is partly through buildings or foliage or totally through tunnels or bridges, as well as GNSS multipath effects [22] may however limit the availability or at least the precision and confidence of a GNSS signal. If no other absolute means of localization is available at this point, the calculated vehicle pose will drift away from its actual position. In case a precise GNSS lock with high confidence returns, the calculated vehicle pose will jump back to its actual position in a short time.

We model this behavior with a Ramp function $R(t)_n$ that generates a uniformly distributed interval between 4s and 10s and interpolates in this interval between no offset and

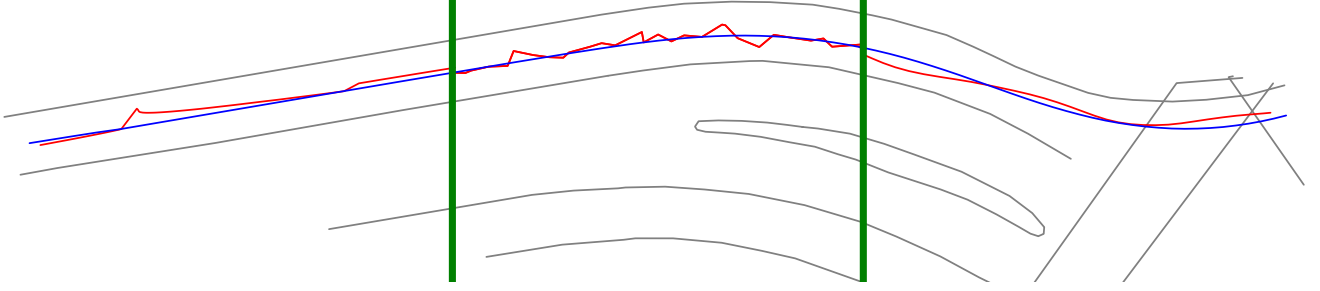


Fig. 3: Qualitative example with ground truth (blue) and noisy localization (red) with Ramp noise (left), Gaussian noise (middle) and Perlin noise (right).

a uniformly distributed translation offset T_n between 0 and ϵ_L as well as a uniformly distributed angular offset θ_n between $-\epsilon_R$ and ϵ_R around the yaw axis. The direction α_n of the translation offset is uniformly distributed between 0 and 360° . The Ramp function is called again as soon as the previous interval is exceeded:

$$\begin{pmatrix} x_\eta(t) \\ y_\eta(t) \\ \theta_\eta(t) \end{pmatrix} = \begin{pmatrix} x_{gt}(t) \\ y_{gt}(t) \\ \theta_{gt}(t) \end{pmatrix} + \begin{pmatrix} \cos(\alpha_n)T_n \\ \sin(\alpha_n)T_n \\ \theta_n \end{pmatrix} R_n(t) \quad (1)$$

$$R_n(t) = \frac{t - t_n}{t_{n+1} - t_n}; t_{n+1} > t \geq t_n \quad (2)$$

$$t_{n+1} \sim \mathcal{U}(t_n + 4s, t_n + 10s); \alpha_n \sim \mathcal{U}(0, 360^\circ) \quad (3)$$

$$T_n \sim \mathcal{U}(0, \epsilon_L); \theta_n \sim \mathcal{U}(-\epsilon_R, \epsilon_R). \quad (4)$$

Fig. 3 shows an example of the noisy localization on the left.

2) *Gaussian noise*: One of the simplest ways of obtaining a localization is using the output from an absolute localization source such as GNSS without filtering. This would provide us with a somewhat noisy output around the vehicle's actual position.

We model this by applying a truncated Gaussian distribution $\mathcal{N}_{[\cdot]}$ with a mean of 0 as an offset for both the translation T_t and the angular case θ_t . The direction of the translation offset is uniformly distributed between 0 and 180° :

$$\begin{pmatrix} x_\eta(t) \\ y_\eta(t) \\ \theta_\eta(t) \end{pmatrix} = \begin{pmatrix} x_{gt}(t) \\ y_{gt}(t) \\ \theta_{gt}(t) \end{pmatrix} + \begin{pmatrix} \cos(\alpha_n)T_t \\ \sin(\alpha_n)T_t \\ \theta_t \end{pmatrix} \quad (5)$$

$$T_t \sim \mathcal{N}_{[\cdot]}(\mu = 0, \sigma_L^2, -\epsilon_L, \epsilon_L) \quad (6)$$

$$\theta_t \sim \mathcal{N}_{[\cdot]}(\mu = 0, \sigma_R^2, -\epsilon_R, \epsilon_R) \quad (7)$$

$$\alpha_t \sim \mathcal{U}(0^\circ, 180^\circ). \quad (8)$$

Fig. 3 shows an example of the noisy localization in the middle.

3) *Perlin noise*: In addition to blocked or raw GNSS signals, we can also obtain a stable but poor GNSS signal with some noise in it. This results in a smooth, wavelike path, as opposed to a GNSS drift or zigzagging GPS trajectory. This phenomenon can, for instance, be observed in the context of badly adjusted tracking in case an improperly adjusted Kalman filter is employed.

To model this behavior, we apply Perlin noise [23] to the trajectory points and the vehicle heading. Therefore, we model

the noise for longitude and lateral coordinate and the vehicle heading each with a random generator to generate different Perlin noise functions. To control the structure of the noise we use two parameters. The first one is the *octave* parameter, which specifies the number of rectangles in each $[0,1]$ range. This parameter is employed to define the frequency of the noise and, consequently, its degree of fineness. Given that the sampling of the points, and thereby the smoothness of the applied Perlin noise, is influenced by the vehicle's speed and GNSS sampling, we introduce the step length parameter, denoted by γ . By multiplying the x - and y -coordinates of the trajectory with the step length parameter γ we can vary the smoothness of the noise:

$$\begin{pmatrix} x_\eta(t) \\ y_\eta(t) \\ \theta_\eta(t) \end{pmatrix} = \begin{pmatrix} x_{gt}(t) \\ y_{gt}(t) \\ \theta_{gt}(t) \end{pmatrix} + \begin{pmatrix} P_x(x_t \cdot \gamma, y_t \cdot \gamma) \\ P_y(x_t \cdot \gamma, y_t \cdot \gamma) \\ P_\theta(x_t \cdot \gamma, y_t \cdot \gamma) \end{pmatrix}. \quad (9)$$

In our experiments, we set γ to 1000 and *octave* to 10 to obtain smooth wavering trajectories. The result of a trajectory with Perlin noise is shown on the right side in Fig. 3.

For the parameter selection of all noise types, we plotted noisy trajectories with different parameter sets on aerial images and selected those parameter sets most fitting to our experience with localization error patterns.

4) *Heading correction*: A resulting heading direction that is majorly different from the current direction of travel would contradict common vehicle dynamic models such as the linear one-track model. We therefore include the option to correct the vehicle heading accordingly:

$$\theta_{\text{noise}} = \theta_{\text{gt}} + \angle \Delta \mathbf{p}_{\text{gt}} \Delta \mathbf{p}_{\text{noise}} \quad (10)$$

Since the Gaussian noise case is aimed to explore the usage of raw sensor data for pose acquisition in contrast to a more sophisticated model-based filtering approach, the effects of the heading correction are only investigated for Ramp and Perlin noise cases.

5) *Partly altered training data*: In light of the aforementioned factors, localization noise may only be present in a limited section of the data at hand. It is therefore of interest to investigate the influence of only partially altered training data on the model's performance. This is modeled by applying the

TABLE I: Comparison between prediction results for the noise types Ramp, Gaussian, and Perlin evaluated using Average Precision (AP). As noise parameters, we defined the maximum translation error ϵ_L , maximum angular error ϵ_R , for the Gaussian noise case standard deviation in translation σ_L and angular σ_R direction, noise ratio NR as the percentage of altered ground truth, and heading correction HC as correction to the now altered driving direction.

Experiment	Noise parameters						AP _{dsh}	AP _{sol}	AP _{bou}	AP _{cen}	AP _{ped}	mAP
	ϵ_L	σ_L	ϵ_R	σ_R	NR	HC						
Baseline B	-	-	-	-	-	-	36.7	54.4	49.6	48.3	40.0	45.8
Ramp R_1	2 m	-	1°	-	50 %	✓	34.8	52.1	46.0	46.1	36.5	43.1
Ramp R_2	2 m	-	0°	-	100 %	✗	32.0	49.0	46.5	44.3	33.6	41.1
Ramp R_3	2 m	-	0°	-	100 %	✓	30.6	46.4	43.7	42.7	33.1	39.3
Ramp R_4	2 m	-	1°	-	100 %	✓	29.8	45.6	44	43.1	31.8	38.9
Ramp R_5	1 m	-	0.5°	-	100 %	✓	33.9	50.7	46.0	46.6	37.5	43.0
Gaussian G_1	2 m	0.5 m	0°	0°	100 %	✗	33.4	52.4	46.5	40.4	37.6	42.1
Gaussian G_2	2 m	0.5 m	0.3°	1°	100 %	✗	33.9	53.3	47.4	44.7	37.2	43.3
Gaussian G_3	2 m	0.5 m	3°	10°	100 %	✗	25.2	36.4	41.8	31.2	35.4	34.0
Perlin P_1	0 m	-	0.5°	-	100 %	✗	38.3	55.4	47.7	48.1	39.2	45.7
Perlin P_2	1 m	-	0°	-	100 %	✓	29.4	42.8	42.0	39.8	34.9	37.8
Perlin P_3	2 m	-	0°	-	100 %	✓	17.2	29.5	31.9	25.6	30.8	27.0
Perlin P_4	2 m	-	0.5°	-	100 %	✓	17.6	31.5	32.5	27.2	30.5	27.9

previously introduced noise types to only a percentage NR of the ground truth while leaving the remaining unaltered.

B. Distance-aware map construction metric

MapTR [1], [2], VectorMapNet [3] and M3TR [12] use the average precision (AP) as an evaluation metric and a perception range of [-15m,15m] for the X-axis and [-30m,30m] for the Y-axis. For the calculation of the AP, the chamfer distance with the thresholds $T = \{0.5m, 1.0m, 1.5m\}$ is used for matching between prediction and ground truth. Then, the final AP is calculated as the average across all thresholds. A problem of this evaluation metric is that spatial relations between the vehicle and the predicted object are ignored. From the perspective of a vehicle, it is more challenging to predict the precise location of objects at a considerable distance than those in the immediate vicinity. Furthermore, in the autonomous driving task, those objects that are closer to the vehicle have a higher priority to be predicted correctly and precisely, because objects that are farther away can be predicted more precisely in future time steps when they get closer to the vehicle.

To address this gap of missing spatial relations between vehicle and prediction, we introduce a new distance-aware evaluation metric for HD map construction. Analog to [1], [2], [3], [4] the chamfer distance is used to assign the prediction to the ground truth elements.

After that, annuli \mathcal{D} , from now on referred to as rings, with equal width are calculated centered around the actual position of the vehicle. We process each ring individually. For each ring, we iterate over all assigned prediction and ground truth element pairs. At this point, we upsample these elements linearly with a maximum point-to-point distance of 1m. Now we differentiate:

- Element pairs, for which at least one element does not include points with overlap with the ring’s area are discarded at this point.

- For element pairs that only consist of points overlapping with the ring’s area the chamfer distance between the element pair is calculated and added to the results list.
- For element pairs that consist of both points overlapping with the ring and points outside the ring, polylines are interpolated linearly at ring borders to include a point right at the ring borders. We now discard all points that do not overlap with the ring area and separate polylines into multiple polylines at ring borders.

Since each element (ground truth or prediction) is now represented by multiple sub-elements, we need to calculate an assignment between ground truth and prediction sub-elements within this subset. We again use chamfer distance for this assignment. At this point, we set an upper bound with the radius of the ring’s outer circle for sub-elements to be assigned. We add the value of the chamfer distance between the assigned sub-element pairs to the results list.

Fig. 1 shows accepted (sub-) elements in color with rejected polylines in gray for an example ring and ground truth sample. The results list entries are best displayed in a statistical representation such as a box plot.

The formula for the distance-aware chamfer distance CD_{\odot} for a GT element \mathcal{S}_1 , the assigned prediction \mathcal{S}_2 , and the distance ring \mathcal{D} is written in Eq. (11) and Eq. (12).

$$\overline{CD}_{\odot}(\mathcal{S}_1, \mathcal{S}_2, \mathcal{D}) = \frac{1}{\mathcal{S}_1} \sum_{p \in \mathcal{S}_1 \cap \mathcal{D}} \min_{q \in \mathcal{S}_2 \cap \mathcal{D}} \|p - q\|_2 \quad (11)$$

$$CD_{\odot}(\mathcal{S}_1, \mathcal{S}_2, \mathcal{D}) = \frac{\overline{CD}_{\odot}(\mathcal{S}_1, \mathcal{S}_2, \mathcal{D}) + \overline{CD}_{\odot}(\mathcal{S}_2, \mathcal{S}_1, \mathcal{D})}{2} \quad (12)$$

This metric definition allows a real comparison of the precision of the predicted elements in terms of a geometric distance, ignoring multiple or missing predictions, which are covered in the AP metric.

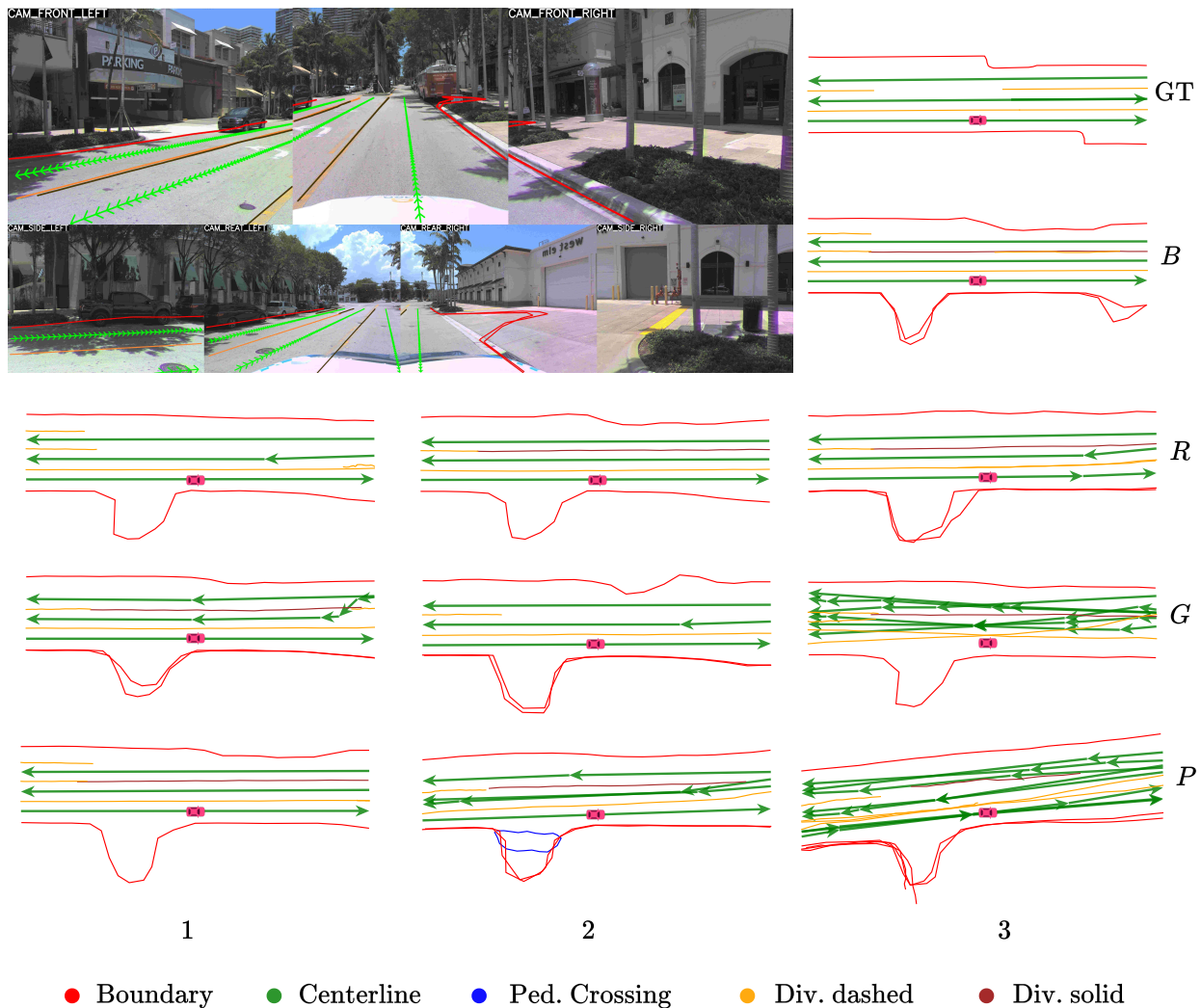


Fig. 4: Qualitative prediction results for the Baseline B (trained without noisy GT labels), Ramp $R_1 - R_3$, Gaussian $G_1 - G_3$, and Perlin $P_1 - P_3$ for the camera input (top left, Baseline results are projected into the image) and the ground truth map GT .

IV. EVALUATION

A. Experimental setup

We conduct our experiments on the Argoverse 2 dataset [6]. To avoid geographical overlap between train, validation, and test sets, we implement the geographical split proposed by Lilia et al. [24]. As the image backbone, we use ResNet50 [25] and the hyperparameters and experimental setup mostly from Vanilla MapTRv2 [2] for all models, whereby we follow [12] for the geographical split and prediction of different divider types.

We apply the noise types introduced in Section III-A only to the training split at label generation time. The labels generated therefore contain a shifted and/or turned local "cutout" of the global map. At training time, the current model only "sees" the same set of altered labels. The test and validation split remain unaltered.

Our focus lies on exploring a broader set of parameters instead of reaching full convergence. Therefore, we find a training over a total of 12 epochs sufficient, also limiting the overall computational requirements. We evaluate using the AP in Table I as well as our newly defined distance-aware evaluation metric.

We present the effect of noise applied to the train split and evaluate the respective model's performance against the validation ground truth in Fig. 5, Fig. 6, Fig. 7 and Fig. 8 as a selection of our performed experiments.

Experiments and their relevant noise parameters can be referenced to each other through their annotation, as defined in the first column of Table I. We also examined the Precision during the assignment for all experiments, but there were no substantial changes regarding the Baseline and it remains stable at 0.3.

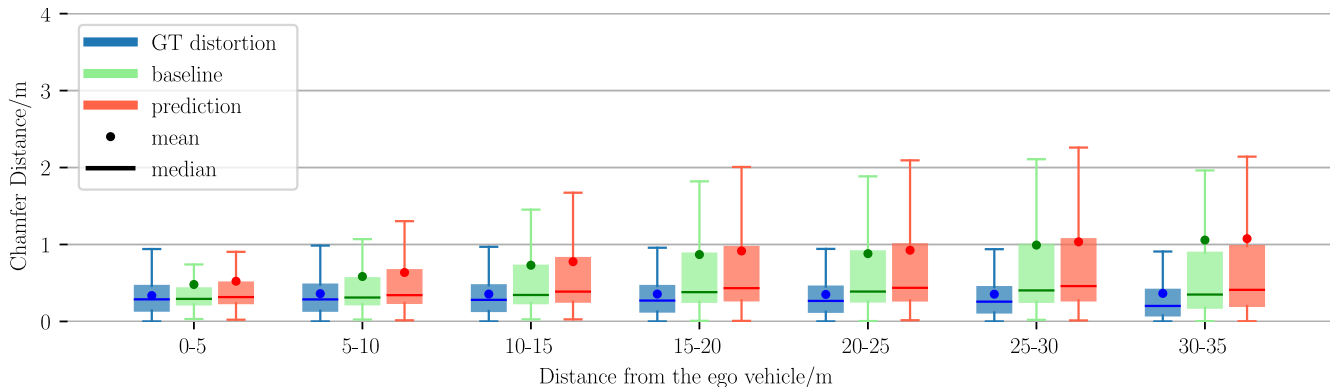


Fig. 5: Gaussian G_1 (GT distortion and prediction) and Baseline B_1

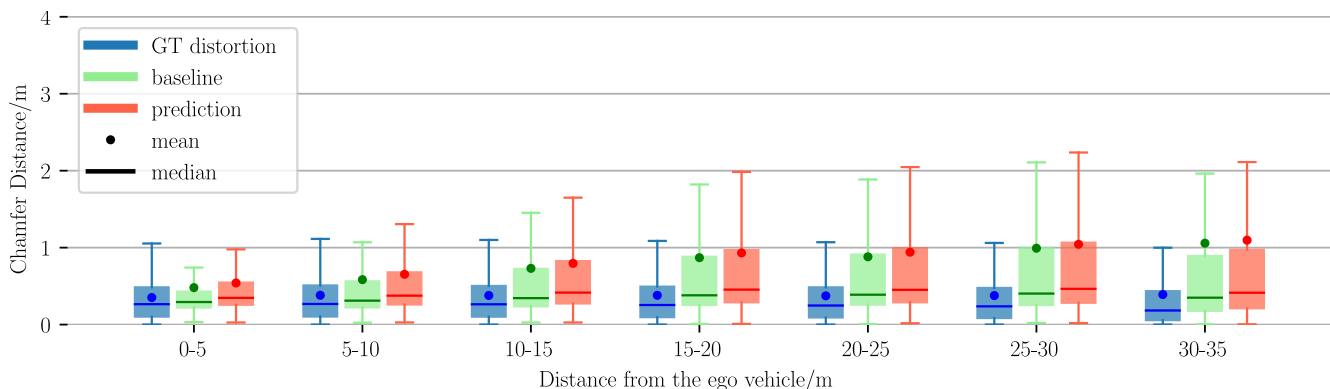


Fig. 6: Ramp R_2 (GT distortion and prediction) and Baseline B_1

B. Qualitative analysis

To present prediction artifacts typical to specific noise scenarios we include Fig. 4 as a comparison between the Ground Truth GT , Baseline B , Ramp R_{1-3} , Gaussian G_{1-3} and Perlin P_{1-3} .

Slight label errors as shown in Ramp R_1 , Gaussian G_1 , and Perlin P_1 produce comparable predictions to the Baseline B model. Medium levels of label errors like in Ramp R_2 , Gaussian G_2 , and Perlin P_2 will still manage to maintain the overall structure and therefore the logic behind the scene albeit with increased levels of warping. Additionally, the Perlin P_2 model starts to get confused by the noise and predicts wrong map elements, such as the pedestrian crossing or double centerline detections at the edge of the perception range.

With increased label error, models tend to output a higher amount of multiple predictions for the same map element, beginning with centerline predictions, see Gaussian G_3 . At even higher label errors, multiple predictions for other object classes occur more often and the entire scene loses its overall structure and orientation, see Perlin P_3 .

C. Temporal aspect

While all of our noise cases are motivated through scenarios that can be found in real-world applications, they can in general be divided into two categories. While the Perlin

and Ramp case (within the Ramp interval) are temporally consistent, the Gaussian case is not.

When comparing R_2 and G_1 , which share comparable levels of label distortion according to Fig. 5 and Fig. 6, the resulting prediction evaluation turns out not majorly different according to both the mAP metric with 41.1 and 42.1 as well as our distance aware metric.

Given that the architecture of MapTRv2 [2] does not incorporate a temporal aspect, this behavior matches the expectations. We would expect a model considering the temporal aspect such as [4] or [5] to provide better performance for Ramp or Perlin noise for the same level of distortion.

D. Partly altered training data

In terms of only partially altered training data, the experiment Ramp R_1 is conducted as illustrated in Table I. In comparison to Ramp R_4 and Baseline B , concerning the percentage of data altered, Ramp R_1 demonstrates a disproportionately superior performance in terms of mAP, exhibiting comparable performance to the Baseline B . In contrast, Ramp R_4 demonstrates a greater performance degradation, exceeding twofold, when the noise ratio is doubled from 50% to 100%. This finding indicates that the model's performance is enhanced by the presence of correct labels and its capacity to adapt to noisy labels is augmented when correct labels are available in the dataset.

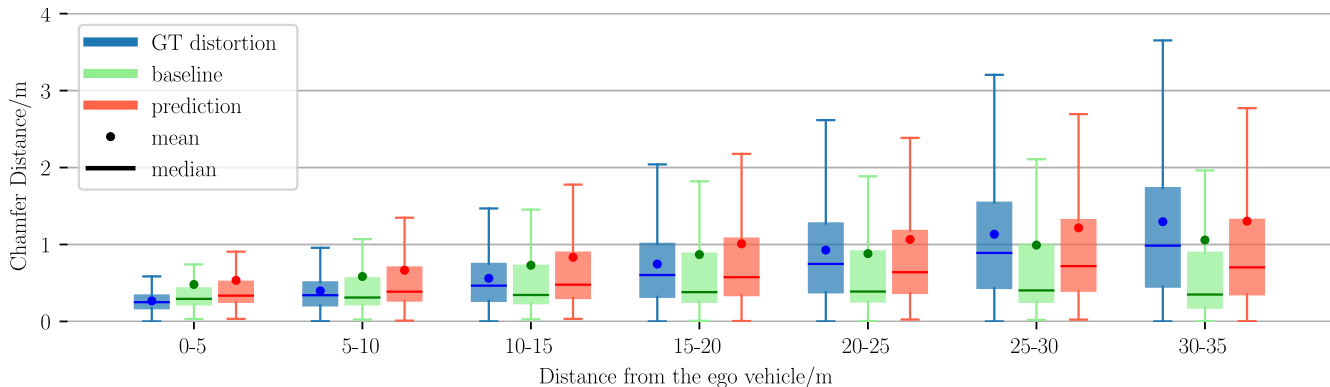


Fig. 7: Perlin P_2 (GT distortion and prediction) and Baseline B_1

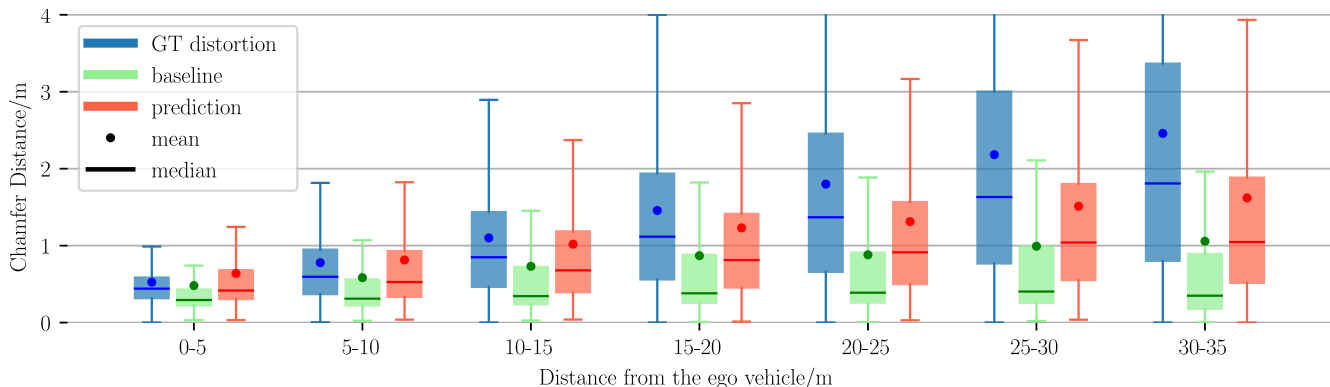


Fig. 8: Perlin P_3 (GT distortion and prediction) and Baseline B_1

E. Influence of heading correction

A special focus of this work lies in the difference in applying a purely translational offset in comparison to an angular error.

Throughout this work, we recognized that including a heading correction HC using a pragmatic noise parameter set as shown in Table I has a greater effect on both the imposed error through the altered training label at an increased distance from the vehicle and the resulting model’s performance in terms of mAP.

When analyzing the induced error for the training of Perlin P_2 and P_3 , as shown in Fig. 7 and Fig. 8, both result in an almost linear relationship between mean/median error in chamfer distance and distance from ego pose, a relationship expected from a predominantly angular error. Additionally, the error is effectively twofold with a doubling in ϵ_L . Relative to this, the error induced in Ramp R_2 and Gaussian G_1 as shown in Fig. 5 and Fig. 6 respectively as a purely translational error is considerably less severe.

Focusing on the resulting model’s prediction error of Perlin P_2 and P_3 , as shown in Fig. 7 and Fig. 8, the error, again in terms of mean/median, increases less severe than altered training data evaluation would suggest. In general, for both cases the statistical magnitude of the induced error during training is greatly reduced with regard to the model’s

performance. Furthermore, the difference in mAP as in Table I suggests a much steeper difference in performance, a property justifiably with the threshold-based definition of mAP.

V. CONCLUSIONS

Based on real-world problem cases, we model three different localization noise scenarios, Ramp, Gaussian and Perlin noise, which we apply to the geographical training split of the Argoverse 2 dataset. We train individual models based on the MapTRv2 architecture for a set of different pragmatically chosen noise parameters.

Besides the common mAP metric and qualitative analysis we introduce a novel detection to ego pose distance-aware metric, that allows for a more structured analysis of our altered training labels as well as model predictions, which we evaluate against the validation splits of unaltered ground truth.

Here, we show the stronger reliance on a low angular error compared to a translational error for adequate map perception performance, especially at higher distances from the ego vehicle. This angular error is applied directly in some of your noise cases, in others it is created by the heading correction. This we employ to correct the changed direction of travel caused by our introduced translational error. The negative consequence of heading correction on the model’s performance cannot be understated at this point and should be considered during localization filter design.

Since one of our localization noise patterns, Gaussian noise, does not produce a temporally consistent localization error, we show that, based on otherwise statistically similar label input, the models perform very comparable. Models with temporal dependencies in their architecture may react differently though.

By altering only a percentage of the ground truth, we show the model's performance to be enhanced beyond what this percentage would infer by the presence of correct labels. Having few bad sections in an otherwise good localization during dataset recording should therefore still yield good model performance.

Through our qualitative analysis, we deliver an assessment regarding the level of localization noise applied and the model no longer producing adequate map perception performance. Whereas smaller levels of localization errors can be largely compensated by the model, medium levels still produce logically coherent results albeit with increased levels of warping. In a multi-drive fleet data scenario, it should still be possible to compensate for these effects through aggregation of multiple drives. At high levels of localization error, the overall structure of the scene gets lost; such scenarios should be avoided.

ACKNOWLEDGMENTS

This work results from the just better DATA (jbDATA) project supported by the German Federal Ministry for Economic Affairs and Climate Action of Germany (BMWK) and the European Union, grant number 19A23003H and was supported by Helmholtz AI computing resources (HAICORE) of the Helmholtz Association's Initiative and Networking Fund through Helmholtz AI.

REFERENCES

- [1] B. Liao, S. Chen, X. Wang, T. Cheng, Q. Zhang, W. Liu, et al., "Maptr: Structured modeling and learning for online vectorized hd map construction," in *International Conference on Learning Representations*, 2023.
- [2] B. Liao, S. Chen, Y. Zhang, B. Jiang, Q. Zhang, W. Liu, et al., "Maptrv2: An end-to-end framework for online vectorized hd map construction," *International Journal of Computer Vision*, pp. 1–23, 2024.
- [3] Y. Liu, T. Yuan, Y. Wang, Y. Wang, and H. Zhao, "Vectormapnet: End-to-end vectorized hd map learning," ser. ICML'23, Honolulu, Hawaii, USA: JMLR.org, 2023.
- [4] J. Chen, Y. Wu, J. Tan, H. Ma, and Y. Furukawa, "MapTracker: Tracking with Strided Memory Fusion for Consistent Vector HD Mapping," in *Computer Vision – ECCV 2024*, A. Leonardis, E. Ricci, S. Roth, O. Russakovsky, T. Sattler, and G. Varol, Eds., Cham: Springer Nature Switzerland, 2025, pp. 90–107, ISBN: 978-3-031-72658-3.
- [5] S. Wang, F. Jia, W. Mao, Y. Liu, Y. Zhao, Z. Chen, et al., "Stream query denoising for vectorized hd-map construction," in *Computer Vision – ECCV 2024: 18th European Conference, Milan, Italy, September 29–October 4, 2024, Proceedings, Part XIX*, Milan, Italy: Springer-Verlag, 2024, pp. 203–220, ISBN: 978-3-031-72654-5.
- [6] B. Wilson, W. Qi, T. Agarwal, J. Lambert, J. Singh, S. Khandelwal, et al., "Argoverse 2: Next generation datasets for self-driving perception and forecasting," in *Proceedings of the Neural Information Processing Systems Track on Datasets and Benchmarks (NeurIPS Datasets and Benchmarks 2021)*, 2021.

- [7] H. Caesar, V. Bankiti, A. H. Lang, S. Vora, V. E. Liong, Q. Xu, et al., "Nuscenes: A multimodal dataset for autonomous driving," in *2020 IEEE/CVF Conference on Computer Vision and Pattern Recognition, CVPR 2020, Seattle, WA, USA, June 13-19, 2020*, Computer Vision Foundation / IEEE, 2020, pp. 11 618–11 628.
- [8] N. Carion, F. Massa, G. Synnaeve, N. Usunier, A. Kirillov, and S. Zagoruyko, "End-to-End Object Detection with Transformers," in *Computer Vision – ECCV 2020*, A. Vedaldi, H. Bischof, T. Brox, and J.-M. Frahm, Eds., Cham: Springer International Publishing, 2020, pp. 213–229, ISBN: 978-3-030-58452-8.
- [9] T. Yuan, Y. Liu, Y. Wang, Y. Wang, and H. Zhao, "Streammapnet: Streaming mapping network for vectorized online hd map construction," in *Proceedings of the IEEE/CVF Winter Conference on Applications of Computer Vision (WACV)*, Jan. 2024, pp. 7356–7365.
- [10] K. Z. Luo, X. Weng, Y. Wang, S. Wu, J. Li, K. Q. Weinberger, et al., "Augmenting lane perception and topology understanding with standard definition navigation maps," in *2024 IEEE International Conference on Robotics and Automation (ICRA)*, 2024, pp. 4029–4035.
- [11] S. Zeng, X. Chang, X. Liu, Z. Pan, and X. Wei, *Driving with prior maps: Unified vector prior encoding for autonomous vehicle mapping*, 2024. arXiv: 2409.05352 [cs.CV].
- [12] F. Immel, R. Fehler, F. Bieder, J.-H. Pauls, and C. Stiller, *M3tr: Generalist hd map construction with variable map priors*, 2024. arXiv: 2411.10316 [cs.CV].
- [13] C. G. Northcutt, A. Athalye, and J. Mueller, "Pervasive label errors in test sets destabilize machine learning benchmarks," in *Proceedings of the 35th Conference on Neural Information Processing Systems Track on Datasets and Benchmarks*, Dec. 2021.
- [14] H. Li, Z. Wu, C. Zhu, C. Xiong, R. Socher, and L. S. Davis, "Learning from noisy anchors for one-stage object detection," in *Proceedings of the IEEE/CVF Conference on Computer Vision and Pattern Recognition (CVPR)*, Jun. 2020.
- [15] Z. Chen, Z. Li, S. Wang, D. Fu, and F. Zhao, "Learning from noisy data for semi-supervised 3d object detection," in *Proceedings of the IEEE/CVF International Conference on Computer Vision (ICCV)*, Oct. 2023, pp. 6929–6939.
- [16] B. Adhikari, J. Peltomäki, S. B. Germe, E. Rahtu, and H. Huttunen, "Effect of Label Noise on Robustness of Deep Neural Network Object Detectors," in *Computer Safety, Reliability, and Security. SAFECOMP 2021 Workshops*, I. Habli, M. Suján, S. Gerasimou, E. Schoitsch, and F. Bitsch, Eds., Cham: Springer International Publishing, 2021, pp. 239–250, ISBN: 978-3-030-83906-2.
- [17] A. Freire, L. H. d. S. Silva, J. V. R. d. Andrade, G. O. A. Azevedo, and B. J. T. Fernandes, "Beyond clean data: Exploring the effects of label noise on object detection performance," *Knowledge-Based Systems*, vol. 304, p. 112 544, 2024, ISSN: 0950-7051.
- [18] H. Zhu, C. Xu, W. Yang, R. Zhang, Y. Zhang, and G.-S. Xia, *Robust tiny object detection in aerial images amidst label noise*, 2024. arXiv: 2401.08056 [cs.CV].
- [19] T. Beemelmans, Q. Zhang, C. Geller, and L. Eckstein, "Multicorrupt: A multi-modal robustness dataset and benchmark of lidar-camera fusion for 3d object detection," in *2024 IEEE Intelligent Vehicles Symposium (IV)*, 2024, pp. 3255–3261.
- [20] X. Hao, M. Wei, Y. Yang, H. Zhao, H. Zhang, Y. Zhou, et al., "Is your hd map constructor reliable under sensor corruptions?" *arXiv preprint arXiv:2406.12214*, 2024.
- [21] P. Rieker and T. Schunck, "Zur fahrmechanik des gummibereiften kraftfahrzeugs," *Ingenieur-Archiv*, vol. 11, pp. 210–224, 1940.
- [22] T. Kos, I. Markežić, and J. Pokrajčić, "Effects of multipath reception on gps positioning performance," *Proceedings ELMAR-2010*, pp. 399–402, 2010.
- [23] K. Perlin, "Improving noise," in *Proceedings of the 29th Annual Conference on Computer Graphics and Interactive Techniques*, ser. SIGGRAPH '02, San Antonio, Texas: Association for Computing Machinery, 2002, pp. 681–682, ISBN: 1581135211.
- [24] A. Lilja, J. Fu, E. Stenborg, and L. Hammarstrand, "Localization is all you evaluate: Data leakage in online mapping datasets and how to fix it," in *Proceedings of the IEEE/CVF Conference on Computer Vision and Pattern Recognition (CVPR)*, Jun. 2024, pp. 22 150–22 159.
- [25] K. He, X. Zhang, S. Ren, and J. Sun, "Deep residual learning for image recognition," in *Proceedings of the IEEE Conference on Computer Vision and Pattern Recognition (CVPR)*, Jun. 2016, pp. 770–778.